Medical Physics
The International Journal of Medical Physics Research and Practice

Toward adaptive radiotherapy for head and neck patients: Feasibility study on using CT-to-CBCT deformable registration for "dose of the day" calculations

Catarina Veiga, Jamie McClelland, Syed Moinuddin, Ana Lourenço, Kate Ricketts, James Annkah, Marc Modat, Sébastien Ourselin, Derek D'Souza, and Gary Royle

Citation: Medical Physics **41**, 031703 (2014); doi: 10.1118/1.4864240
View online: http://dx.doi.org/10.1118/1.4864240
View Table of Contents: http://scitation.aip.org/content/aapm/journal/medphys/41/3?ver=pdfcov
Published by the American Association of Physicists in Medicine

Toward adaptive radiotherapy for head and neck patients: Feasibility study on using CT-to-CBCT deformable registration for "dose of the day" calculations

Catarina Veiga[a)]
Radiation Physics Group, Department of Medical Physics and Bioengineering, University College London, London WC1E 6BT, United Kingdom

Jamie McClelland
Centre for Medical Image Computing, Department of Medical Physics and Bioengineering, University College London, London WC1E 6BT, United Kingdom

Syed Moinuddin
Department of Radiotherapy, University College London Hospital, London NW1 2BU, United Kingdom

Ana Lourenço, Kate Ricketts, and James Annkah
Radiation Physics Group, Department of Medical Physics and Bioengineering, University College London, London WC1E 6BT, United Kingdom

Marc Modat and Sébastien Ourselin
Centre for Medical Image Computing, Department of Medical Physics and Bioengineering, University College London, London WC1E 6BT, United Kingdom

Derek D'Souza
Department of Radiotherapy Physics, University College London Hospital, London NW1 2PG, United Kingdom

Gary Royle
Radiation Physics Group, Department of Medical Physics and Bioengineering, University College London, London WC1E 6BT, United Kingdom

(Received 8 October 2013; revised 18 January 2014; accepted for publication 21 January 2014; published 19 February 2014)

Purpose: The aim of this study was to evaluate the appropriateness of using computed tomography (CT) to cone-beam CT (CBCT) deformable image registration (DIR) for the application of calculating the "dose of the day" received by a head and neck patient.
Methods: NiftyReg is an open-source registration package implemented in our institution. The affine registration uses a Block Matching-based approach, while the deformable registration is a GPU implementation of the popular B-spline Free Form Deformation algorithm. Two independent tests were performed to assess the suitability of our registrations methodology for "dose of the day" calculations in a deformed CT. A geometric evaluation was performed to assess the ability of the DIR method to map identical structures between the CT and CBCT datasets. Features delineated in the planning CT were warped and compared with features manually drawn on the CBCT. The authors computed the dice similarity coefficient (DSC), distance transformation, and centre of mass distance between features. A dosimetric evaluation was performed to evaluate the clinical significance of the registrations errors in the application proposed and to identify the limitations of the approximations used. Dose calculations for the same intensity-modulated radiation therapy plan on the deformed CT and replan CT were compared. Dose distributions were compared in terms of dose differences (DD), gamma analysis, target coverage, and dose volume histograms (DVHs). Doses calculated in a rigidly aligned CT and directly in an extended CBCT were also evaluated.
Results: A mean value of 0.850 in DSC was achieved in overlap between manually delineated and warped features, with the distance between surfaces being less than 2 mm on over 90% of the pixels. Deformable registration was clearly superior to rigid registration in mapping identical structures between the two datasets. The dose recalculated in the deformed CT is a good match to the dose calculated on a replan CT. The DD is smaller than 2% of the prescribed dose on 90% of the body's voxels and it passes a 2% and 2 mm gamma-test on over 95% of the voxels. Target coverage similarity was assessed in terms of the 95%-isodose volumes. A mean value of 0.962 was obtained for the DSC, while the distance between surfaces is less than 2 mm in 95.4% of the pixels. The method proposed provided adequate dose estimation, closer to the gold standard than the other two approaches. Differences in DVH curves were mainly due to differences in the OARs definition (manual vs warped) and not due to differences in dose estimation (dose calculated in replan CT vs dose calculated in deformed CT).

Conclusions: Deforming a planning CT to match a daily CBCT provides the tools needed for the calculation of the "dose of the day" without the need to acquire a new CT. The initial clinical application of our method will be weekly offline calculations of the "dose of the day," and use this information to inform adaptive radiotherapy (ART). The work here presented is a first step into a full implementation of a "dose-driven" online ART. [http://dx.doi.org/10.1118/1.4864240]

Key words: adaptive radiotherapy, cone-beam CT, deformable image registration, head and neck cancer

1. INTRODUCTION

A radiotherapy treatment starts with the acquisition of a computerized tomography (CT) scan, which is used to plan an individualized treatment for the patient. The treatment is then delivered over several weeks, based on the premise that the anatomy is unchanged since the planning stage. Possible changes are considered by including treatment margins when delineating volumes of interest. Patient positioning verification is performed using image-guidance. Cone-beam CT (CBCT) is a popular imaging method that provides valuable 3D information of the patient in treatment position. However, the imaging quality is inferior compared to CT,[1] resulting in incorrect Hounsfield units (HU) for dose calculations.[2] It is well known that patient's anatomy can vary within a fraction, with swallowing and respiratory motion,[3] and from fraction to fraction, with changes in bladder/bowel filling and tumor shrinkage.[4] The concept of adaptive radiotherapy (ART) suggests a change of paradigm in radiotherapy:[5] the stationary anatomy is replaced by a variable anatomy, by utilizing daily imaging in the radiotherapy process.[6]

ART is a very broad subject and full clinical implementation requires further developments in computational power, image guidance, dose verification, and plan adaptation.[6,7] It is widely accepted that deformable image registration (DIR) algorithms will play a vital role in ART:[8–10] the planning CT (pCT) can be deformed to match the daily anatomy (CBCT) for calculating the "dose of the day," the deformation field can be used for automatic recontouring and the daily dose distributions can be warped back to the pCT for dose summation.[11]

This study is focused on head and neck (HN) patients. Several studies show that HN patients' anatomy changes during the course of the treatment, and that this results in dosimetric changes from the original plan.[4,12,13] It is clear that some patients require at least one replan,[14] but it is not clear which benefits the most from ART and when is the right time for intervention. Currently, in University College London Hospital (UCLH) the decision to replan is based on clinical experience and offline review of CBCTs acquired. A more desirable approach would be to estimate the dose actually received by the patient during treatment ("dose of the day"), and use this dosimetric information to feed the decision-making process.

To calculate the "dose of the day" and assess if the current plan is still acceptable, an image of the patient in treatment position with structures of interest delineated is necessary, and DIR can provide a solution to answer both those needs. We optimized a DIR algorithm implemented at our institution for CT-to-CBCT registrations in HN patients, and investigated its suitability to correctly estimate the "dose of the day" for an intensity modulated radiation therapy (IMRT) treatment. Two other common approaches suggested in the literature to calculate the "dose of the day" are based on image guidance with CT imaging,[15] and direct dose calculations on the CBCT, using pixel correction techniques[16,17] or relative electron density calibration.[18,19] The first increases the dose given to the patient in the image guidance protocols and requires an in-room CT scanner, which is not available in our practice. The second is more limited by the inherent properties of CBCT imaging, such as proneness to motion artifacts, increased noise, reduced contrast, and limited field-of-view (FoV). It also requires delineation of structures of interest, which can be challenging in a CBCT scan.

DIR validation is challenging due to the lack of gold standards in clinical and nonclinical settings.[20] While there is a wide variety of studies assessing the quality of CT-CT deformable registration with patient data,[8,21] for CT-CBCT the studies are scarcer and usually focused on the deformation properties rather than dosimetry.[22–25] In this work we use image inspection, feature-based evaluation, and comparison of dose distributions to assess the suitability of our DIR algorithm implementation for the clinical application of dose calculations in HN patients.

2. METHODS AND MATERIALS

2.A. Patient data acquisition

Retrospective data from five head and neck patients treated in our clinic and referred for possible replan was used in this study (Table I). All patients underwent IMRT with a planned dose of 65 Gy delivered in 30 daily fractions. Patient positioning was assured by appropriate head-rest and a personalized HN and shoulder mask.

The imaging protocol consisted of a planning CT (GE Widebore 16 slice system) with contrast injection, and weekly CBCTs (On-board imaging v1.4, Varian Medical Systems, Palo Alto, CA) acquired in treatment position. The CBCTs were acquired in half-fan mode, full rotation, 110 kVp, 20 mA, 20 ms, with a maximum FoV of 45 cm in diameter, and 16 cm in length. Imaging resolution was $0.977 \times 0.977 \times 2.5$ mm and $0.879 \times 0.879 \times 2$ mm for the CT and CBCT scans, respectively.

The treatment isocenter is usually set to bony anatomy on the identifiable vertebrae and does not represent any

TABLE I. Patient characteristics.

Pt. no.	Age (y)	Gender	Tumor site	TNM classification	Replan (Y/N)	ΔW[a] (%)	ΔV_{ext}[b] (%)	L_{PTV}[c] (mm)	V_{PTV}[d] (%)
1	64	F	Oropharynx	T3N1M0	N	N/A	− 8.5	+15	6.5
2	61	M	Larynx	T3N1M0	Y	+0.4	− 3.5	+8	0.5
3	73	F	Base of the tongue	T4N2cM0	Y	− 1.7	− 4.7	0	0.0
4	60	M	Larynx	T3N0M0	Y	− 4.4	− 12.4	+14	3.0
5	64	M	Pharyngeal wall	T4N2cM0	Y	− 11.7	− 8.6	−26	9.4

[a]ΔW = relative weight variation at plan evaluation.
[b]ΔV_{ext} = relative external volume variation at plan evaluation, in the region imaged by the CBCT.
[c]L_{PTV} = length of the target volume outside the CBCT in the superior/inferior direction, at replan referral.
[d]V_{PTV} = target volume fraction not imaged by the CBCT, at replan referral.

normalization point or high dose region. The CBCT is aligned to the pCT following a standardized online image guidance protocol for isocenter alignment based on manual rigid registration to the cervical spinal vertebrae.

Replanning referral occurred when the CBCT offline review study found the spinal canal or brainstem outside their respective planning organ at risk volume, the external contour decreased more than 5 mm and/or if the immobilization mask was no longer effective. By rigidly aligning the pCT with the CBCT and defining the new body external contour on the pCT based on the CBCT external, target coverage and possible overdosage to organs-at-risk (OARs) were verified, and the decision to replan taken. Four of these patients were replanned midway. A replan CT (rCT) was acquired in the same scanner as the pCT (with contrast) and a new plan built from scratch—a new immobilization mask was necessary but the previous positioning was reproduced as close as possible. Typically the last two weeks of treatment were completed with the new plan.

2.B. NiftyReg

NiftyReg is an open-source registration package implemented by our institution's Centre of Medical Image Computing (http://cmic.cs.ucl.ac.uk/home/software/). While the affine registration implemented in NiftyReg uses a Block Matching-based approach,[26] the deformable registration is a GPU implementation of the popular B-spline Free Form Deformation algorithm using Normalized Mutual Information (NMI) as similarity measure.[27,28]

The registrations were defined by a set of parameters previously optimized to suit the datasets being registered.[29,30] NiftyReg implements a multiresolution approach, and our registrations were carried out using three resolution levels. The B-spline control point grid is placed on the CBCT by aligning the second control point with the centre of the first voxel, as shown in Fig. 1(a). The control point spacing equals five voxels.

Two regularization terms were used: bending energy, which encourages a smoothly varying deformation field,[27] and logarithm of the determinant of the jacobian, which penalizes large volume changes.[31] A folding correction scheme is applied every iteration and to the final deformation field. When folding occurs the correction scheme updates the control point coefficients in the vicinity of folded voxels to try and produce a folding-free transformation.[32] The folding correction scheme ensures the invertibility of the deformation field.

NMI metric with 32 bins was preferred as similarity measure over other popular measures, such as the sum of squared differences (SSD) and global cross-correlation (CC), since it handles not only the nonlinear relationship between CT and CBCT intensities but also the local variations of intensity characteristic of CBCT imaging. The registrations were optimized using a conjugate gradient optimization.

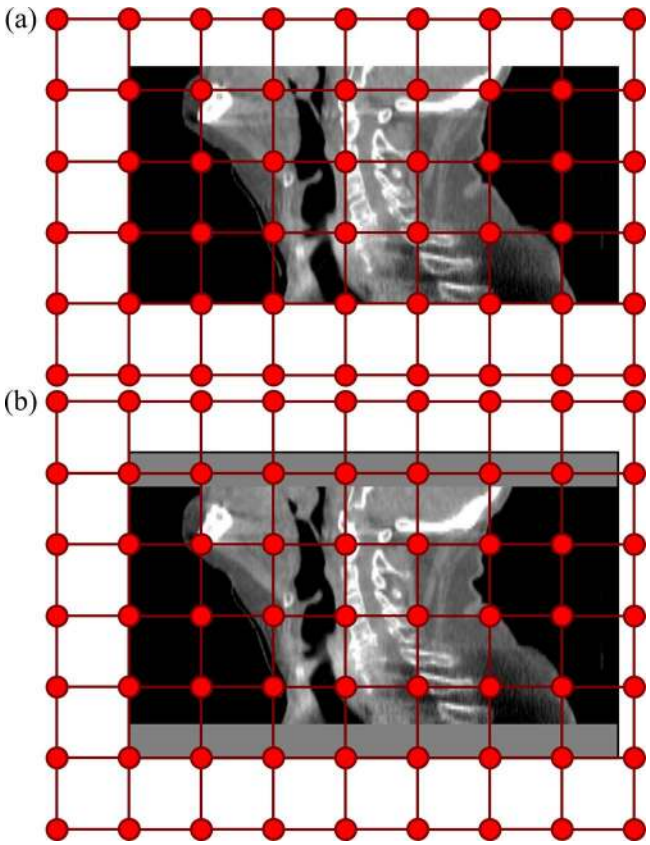

FIG. 1. Standard B-spline control point grid covering: (a) the CBCT volume only and (b) the CBCT volume extended to cover the CT field of view. The second control point position matches the centre of the first voxel of the image.

In our pipeline, the patient images and structures were exported from the treatment planning system (TPS) in DICOM format to a standalone registration workstation. Our registration workstation had an Intel Xeon CPU E25606 (2.13GHz, 12GB RAM) with a NVIDIA Tesla C2070 GPU card (14 multiprocessors, 6 GB dedicated memory). A rigid registration was first applied in order to estimate the global alignment between the pCT and the CBCT. The obtained transformation was then used to initialize the deformable registration. The deformable registrations using images at full resolution ran in approximately 1 min. The output deformation field was used to propagate the contours from the planning CT to the deformed CT, and the results saved in DICOM format. Both the deformed CT and warped structures were then imported back in the TPS for dose calculations.

A well-known issue with CBCT imaging is that the limited FoV often makes the images unusable for treatment planning due to missing patient information.[19] Methods proposed to handle this issue include acquiring two consecutive CBCTs,[33] or directly using pCT slices to extend the CBCT.[11] We estimated the deformation outside the CBCT FoV by continuity, using the initial rigid alignment and the regularization of the deformable registration. The CBCT volume was extended in the superior/inferior direction, to cover the whole CT FoV. Figure 1(b) shows the effect this has on the B-spline control point placement. The deformation outside the FoV was initialized using the rigid alignment. During the registration the transformation is optimized over the whole of the extended volume—as there is no image data to drive the registration outside the field it is purely driven by the constraint terms in these regions. This has the effect of causing a smooth transition between the image driven deformation inside the field of view and the rigid alignment outside the FoV. A good rigid alignment between the pCT and CBCT is then required, and it provides a good approximation mostly in the superior region, as the patient's head moves in a rigid fashion. The superior region is usually the most important due to presence of OARs such as brainstem and parotids. The brainstem only moves rigidly, but the parotids can shrink and migrate,[12] and if not imaged the registration will likely represent the wrong deformation.

2.C. Evaluation of the DIR suitability for "dose of the day" calculations

Two independent tests were performed to assess the appropriateness of our registrations methodology for "dose of the day" calculations in a deformed CT. A geometric evaluation was performed to assess the ability of our DIR method to map identical structures between the CT and CBCT datasets. Features delineated in the pCT were deformed using the output deformation field and compared with the same features manually drawn on the CBCT. We compared the results obtained with those of using a rigid-only registration of the vertebrae. A dosimetric evaluation was performed to evaluate the impact of the registrations errors in the application proposed, to identify the limitations of our out-of-field approximation and assess how our method compares with other approaches.

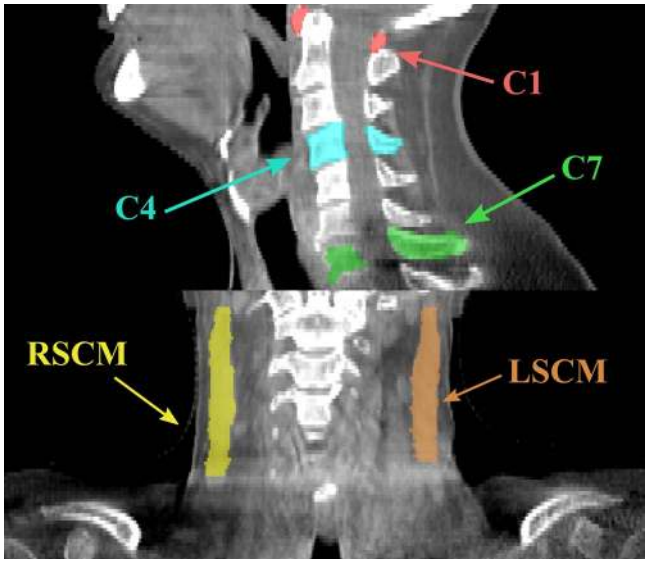

FIG. 2. Features identified on the CT and CBCT images for the geometric evaluation: bony anatomy (vertebrae C1, C4, and C7) and left and right sternocleidomastoid muscles (LSCM and RSCM).

Dose distributions for the same IMRT plan were calculated on the deformed pCT and rCT, and compared. In this second test our method results were compared not only with those from a rigid-only registration of the vertebrae, which approximates our institution's current alignment protocol, but also with dose calculations directly on an calibrated and extended CBCT.[16,17]

2.C.1. Geometric evaluation

The purpose of this test was to assess the DIR ability to align the same anatomical features in CT and CBCT images. For each patient a set of easily identifiable features was drawn by the same clinical expert on both the pCT and the CBCT (Fig. 2). The CBCT used for each patient was the last acquired before replan referral. Due to the noise and low contrast inherent to CBCT imaging, it is difficult to delineate points or delineate structures with confidence and consistency. The features were chosen to be structures that could be unequivocally identified in both scans and that gave an indication of how well the registration accounts for patient positioning errors and weight loss. Vertebrae C1, C4, and C7 were used because they are only subject to rigid motion and cover the length of the cervical spinal canal. External body contour and right and left sternocleidomastoid muscles were used as soft tissue structures. The two muscles are adjacent to the region that contains the neck lymph nodes. Deformation between scans may affect their shape and position, and therefore nodal dose.[34] Typical HN OARs, such as parotids and brainstem, were not considered in this evaluation because they cannot be unequivocally seen in a CBCT scan.

Considering that A and B are the set of voxels that define the volumes of the manual and deformed features while $\tilde{A}$ and $\tilde{B}$ define the corresponding surfaces, three metrics were used to describe the similarity between the features:

- Dice similarity coefficient (DSC)

$$\mathrm{DSC} = \frac{2\,|\mathrm{A} \cap \mathrm{B}|}{|\mathrm{A}| + |\mathrm{B}|}.$$

- Distribution of Euclidean distances between surfaces' points, also known as the distance transform (DT).[21]

$$\mathrm{DT}(\mathbf{a}) = \min(\|\mathbf{a} - \mathbf{b}\|), \qquad \mathbf{a} \in \tilde{\mathrm{A}}, \qquad \forall \mathbf{b} \in \tilde{\mathrm{B}}.$$

  DT was computed bi-directionally and properties of the distribution, such as mean value, were calculated.
- Centroid position error (CoM)

$$\mathrm{CoM} = \|\mathbf{a}_{\mathrm{CoM}} - \mathbf{b}_{\mathrm{CoM}}\|.$$

The metrics presented provide complementary information about the overlap between volumes (DSC), closeness between the surfaces (DT), and spatial positioning of the features (CoM).

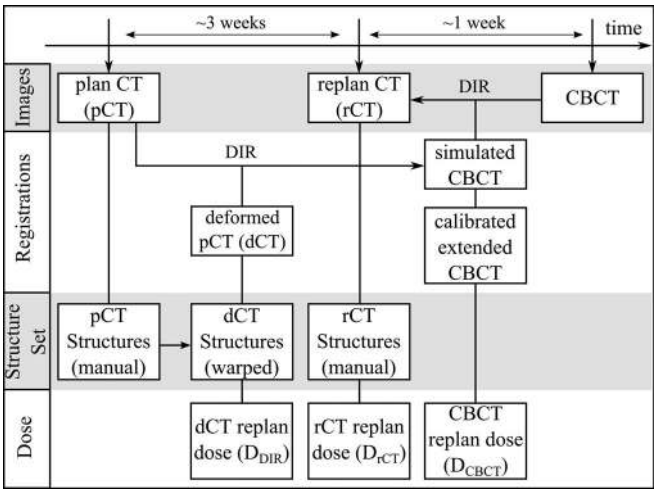

FIG. 3. Diagram of the data and registrations used in the dosimetric evaluation. The structures included in this study were the brainstem, spinal canal, and parotid glands.

2.C.2. Dose comparison

In this second test our aim was to show that we can deform the pCT into an image which is functionally equivalent to a rCT as far as dose calculation is concerned. To test this hypothesis, four different dose distributions were computed for each patient:

(i) recalculated dose in the rCT (D_{rCT}), considered as gold-standard;
(ii) recalculated dose in the deformed pCT, (D_{DIR}), the method we propose;
(iii) recalculated dose in a rigidly aligned pCT (D_{RIG}), our current clinical approach;
(iv) recalculated dose in a calibrated CBCT with superior/inferior extension (D_{CBCT}).

In an ideal situation the rCT and CBCT would have been acquired at the same time, or at least in the same day, so that the two modalities contained the same (or comparable) geometric information. However, using retrospective data such effort is not possible since there is no clinical reason to acquire a CT and a CBCT on the same day. The CBCT used for each patient was the one acquired on the first fraction of the second plan. Since the rCT and following CBCT are not acquired simultaneously, but 5–7 days apart, noticeable changes to the patients' positioning and anatomy can occur between the scans. To minimize the errors in dose estimation due to discrepancies between the rCT and the CBCT, we actually registered the pCT to a simulated CBCT, obtained by deforming the real CBCT to match the rCT. This simulated CBCT is closer to the ideal dataset discussed above. We could have deformed the rCT to match the CBCT instead but we opted against it for three reasons: (i) since we are trying to reproduce the dose calculated on a rCT we did not want to modify the rCT in any way, (ii) the plan isocenter is intrinsically defined in the rCT (further explanation on this point below), and (iii) since CBCT inherently has lower imaging quality possible errors in the deformed CBCT will be less noticeable than similar errors in deforming the rCT. To calculate D_{CBCT} the simulated CBCT values were replaced, pixel by pixel, with CT values and the image was extended in the superior and inferior direction using the corresponding rigidly aligned pCT slices. The relationship between CT and CBCT values was obtained using the Catphan-504 (Phantom Laboratory, NY) calibration phantom. Images of the phantom were acquired and the average HU for each of its constituting materials was calculated for each of the imaging modalities. The conversion curve between CT and CBCT numbers was approximated by a quadratic polynomial. Figure 3 shows the data used and registrations performed for each patient.

Doses were calculated for an IMRT plan using Varian Eclipse External Beam Planning System analytical anisotropic algorithm with the highest available resolution (1 mm). For each patient the same IMRT plan, including beam arrangement, monitor units and fluence maps, were employed. The choice of IMRT plan should be clinically relevant, so a dose distribution the patient was treated with was chosen. The plan chosen to perform the dose calculations was the replan, which was built and optimized in the rCT. This minimizes the issues with the isocenter definition both in the gold-standard, our method and extended CBCT. The uncertainties with isocenter positioning are only an issue when calculating D_{RIG}. The isocenter uncertainty positioning in this case was dealt with by using our clinical protocol for isocenter alignment (described in Sec. 2.A).

The dose distributions were compared considering dose-differences (DD), gamma analysis, and similarity of the 95% isodose region (representing target coverage).

The gamma analysis method compares a reference (D_{ref}) and calculated (D_{cal}) dose distributions using acceptance criteria.[35] It combines two important dose comparison criteria: distance to agreement (Δd_M) and dose-difference (ΔD_M). The gamma quality index (γ) at each point of the calculated dose distribution is given by

$$\gamma(\mathbf{r}_{\mathrm{cal}}) = \min\{\Gamma(\mathbf{r}_{\mathrm{cal}}, \mathbf{r}_{\mathrm{ref}}) \forall \{\mathbf{r}_{\mathrm{ref}}\}\},$$

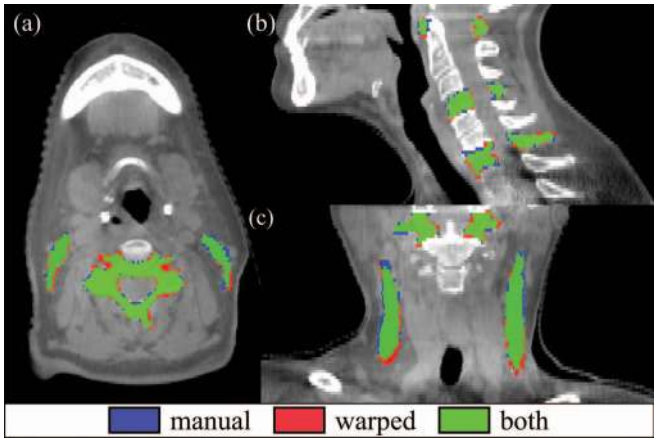

FIG. 4. Geometric matching of manual and warped features overlaid on the CBCT image. Blue corresponds to manual-only, red to warped-only voxels, and green to the region of agreement. The features shown are (from left to right): (a) left sternocleidomastoid muscle (LSCM), C4, and right sternocleidomastoid muscle (RSCM), (b) vertebrae C1, C4, and C7; and (c) LSCM, C1, and RSCM.

where

$$\Gamma(\mathbf{r}_{cal}, \mathbf{r}_{ref}) = \sqrt{\frac{\mathbf{r}^2(\mathbf{r}_{cal}, \mathbf{r}_{ref})}{\Delta d_M^2} + \frac{\delta^2(\mathbf{r}_{cal}, \mathbf{r}_{ref})}{\Delta D_M^2}}$$

with

$$\mathrm{r}(\mathbf{r}_{cal}, \mathbf{r}_{ref}) = |\mathbf{r}_{ref} - \mathbf{r}_{cal}|$$

and

$$\delta(\mathbf{r}_{cal}, \mathbf{r}_{ref}) = D_{ref}(\mathbf{r}_{ref}) - D_{cal}(\mathbf{r}_{cal}).$$

The pass-fail criteria are: $\gamma(\mathbf{r}_{cal}) \leq 1$ the calculation passes, $\gamma(\mathbf{r}_{cal}) > 1$ the calculation fails. The criterion used was $\Delta d_M = 2$ mm and $\Delta D_M = 2\%$.

2.C.3. Propagation of structures and "dose of the day"

The dose analysis was extended to examine the impact within different OARs. In clinical settings, dose volume histograms (DVHs) are routinely used to assess if the plan is appropriate for the patient, by displaying in a concise and comprehensive way the information of dose delivered both to targets and OARs. DVHs were computed using both manually drawn and warped structures of interested. The structures were delineated by the radiographers as part of clinical practice. Complementary to DVH analysis, overlap between OARs manually drawn in the rCT and warped from the pCT was also assessed.

3. RESULTS

3.A. Geometric evaluation

Figure 4 shows a representative example of the matching of manual and warped features. The visual matching of the features is satisfactorily after registration, particularly for complexly shaped features such as the vertebrae.

In Table II we present the mean DSC, DT, and CoM obtained for different types of features. Figure 5 shows the complete information of the distribution of DT values, for different feature and registration types. DIR aligns the features well and considerably better than rigid registration, and the results obtained are more consistent between different structures types. The results obtained are also poorer in soft tissue region than in bone anatomy. Inherent lower soft tissue contrast in the CBCT degrades both the registration accuracy and the quality of manual segmentations. The tail of the DT distribution, and consequently maximum DT values, are thought to be more related with local poor manual segmentation than to registration errors.

3.B. Dose comparison

Overall D_{DIR} matches D_{rCT} well (Fig. 6). The dose similarity results were analyzed based on different regions of the

TABLE II. Mean values (± standard deviation) of dice similarity coefficient (DSC), distance transform (DT), and centroid position error (CoM) obtained using deformable (DIR) and rigid-only (RIG) registrations. The results are grouped by different structure type: external contours, soft tissues (left and right sternocleidomastoid muscles), and bony anatomy (vertebrae C1, C4, and C7).

	External counters		Bony anatomy		Soft tissues		Overall	
Measure	RIG	DIR	RIG	DIR	RIG	DIR	RIG	DIR
DSC	0.945 ± 0.017	0.986 ± 0.001	0.722 ± 0.122	0.846 ± 0.027	0.643 ± 0.143	0.790 ± 0.056	0.733 ± 0.157	0.850 ± 0.076
DT_{2mm}[a] (%)	31.4 ± 8.5	3.6 ± 1.5	20.4 ± 17.7	5.3 ± 3.5	29.2 ± 21.6	8.7 ± 4.9	25.2 ± 18.6	6.2 ± 4.3
DT_{mean}[b] (mm)	1.9 ± 0.8	0.4 ± 0.1	1.4 ± 0.6	0.8 ± 0.1	1.9 ± 1.0	1.0 ± 0.2	1.6 ± 0.8	0.8 ± 0.3
DT_{std}[c] (mm)	2.8 ± 1.1	1.3 ± 0.4	1.2 ± 0.4	0.9 ± 0.2	1.6 ± 0.6	1.1 ± 0.4	1.6 ± 0.8	1.0 ± 0.4
$DT_{95\%}$[d] (mm)	7.8 ± 3.2	2.1 ± 0.3	3.5 ± 1.4	2.4 ± 0.6	4.9 ± 2.3	2.9 ± 1.1	4.7 ± 2.6	2.5 ± 0.9
DT_{max}[e] (mm)	22.0 ± 9.2	18.5 ± 8.2	6.7 ± 2.2	5.5 ± 1.6	10.3 ± 4.1	8.5 ± 4.0	10.4 ± 7.2	8.6 ± 6.2
CoM(mm)	4.4 ± 1.4	0.8 ± 0.3	2.5 ± 1.6	0.8 ± 0.4	3.6 ± 2.8	2.1 ± 0.6	3.2 ± 2.2	1.2 ± 0.8

[a]DT_{2mm} = fraction of the distance transform distribution larger than 2 mm.
[b]DT_{mean} = mean value of the distance transform distribution.
[c]DT_{std} = standard deviation of the distance transform distribution.
[d]$DT_{95\%}$ = 95% percentile of the distance transform distribution.
[e]DT_{max} = maximum value of the distance transform distribution.

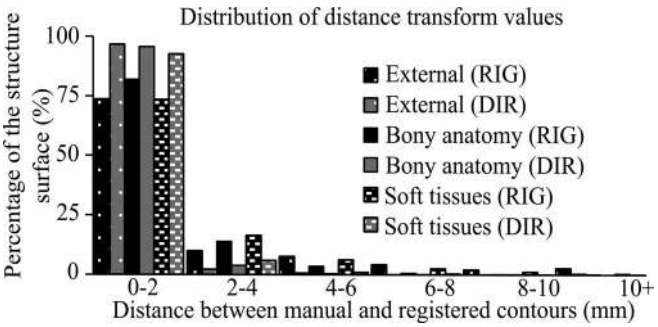

FIG. 5. Distribution of distance transform (DT) values for deformable (DIR, in grey) and rigid only (RIG, in black) registrations. The results are grouped by different structure type: external contours, soft tissues (left and right sternocleidomastoid muscles), and bony anatomy (vertebrae C1, C4, and C7).

patient (Table III), providing evidence of the dose behavior outside the CBCT FoV. D_{DIR} results were better than the D_{RIG} and D_{CBCT} results in all regions, although the major benefits of using D_{DIR} were in the region imaged in the CBCT where most anatomical changes occur and higher dose is delivered.

Target coverage similarity was assessed in terms of the 95%-isodose volumes obtained for D_{DIR}, D_{RIG}, and D_{CBCT} in comparison with D_{rCT}. Our method resulted in a mean value of 0.962 ± 0.015 (range: 0.937–0.978) for the DSC, while the distance between surfaces is less than 2 mm in $95.4\% \pm 5.8\%$ (range: 85.6%–99.8%) of the pixels. For D_{RIG} and D_{CBCT} the values obtained were, respectively, 0.929 ± 0.016 (range: 0.908–0.950), and 0.957 ± 0.011 (range: 0.940–0.971) for DSC, and 79.8 ± 5.3 (range: 73.2%–87.9%) and 93.1 ± 2.7 (range: 88.9%–96.1%) for DT_{2mm}.

For a particular patient the 95%-isodose curve similarity was considerably poorer when compared with the results obtained for the remaining patients. We observed that the CBCT was acquired more superiorly than usual, and so the inferior volume of the high dose region was not fully imaged. As a result, for this particular patient our estimation outside the FoV was not adequate in the inferior direction (where the transformations are not majorly rigid).

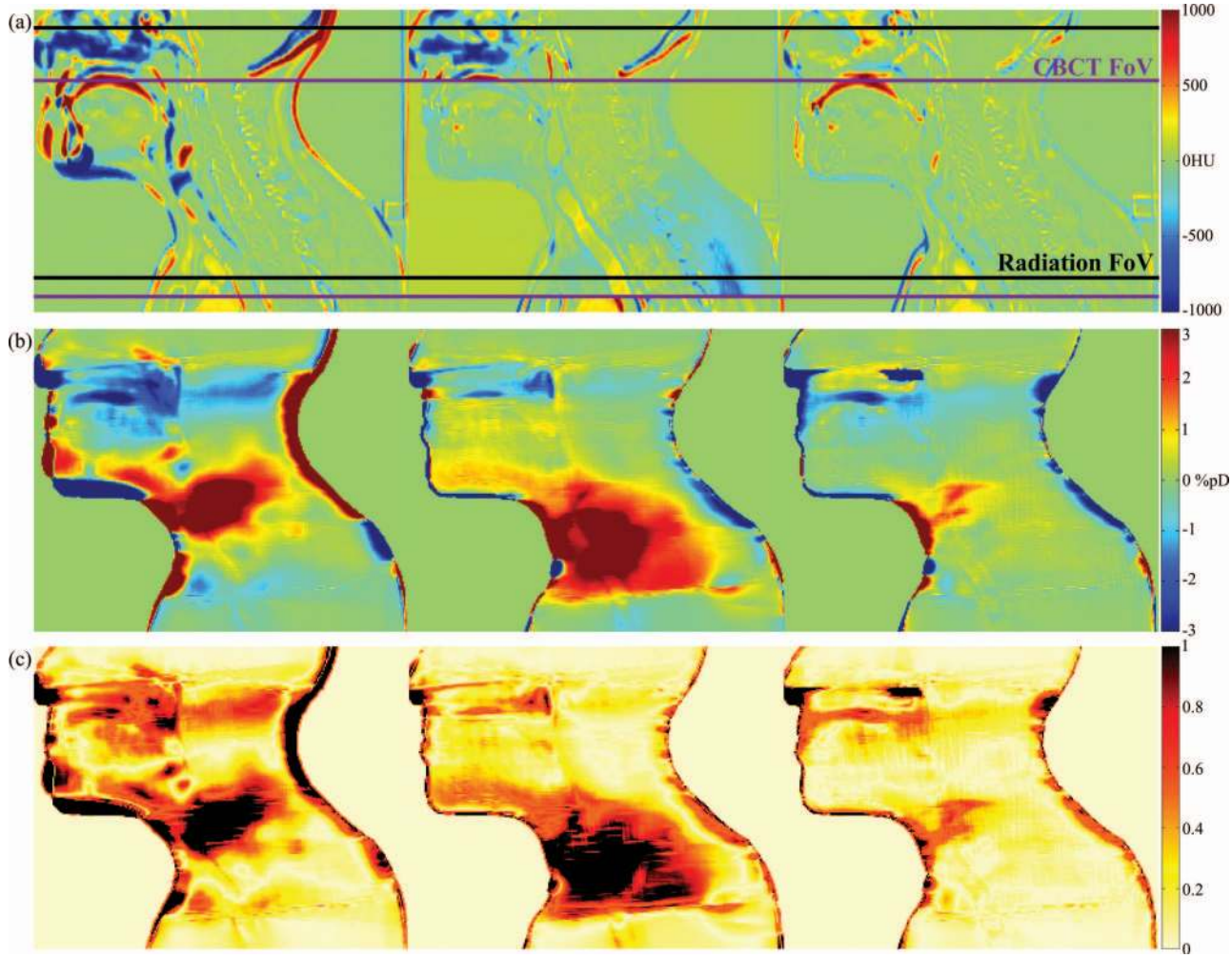

FIG. 6. Rigid (left), extended CBCT (middle), and deformable registrations (right): (a) intensity difference image with the replan CT, (b) dose difference with D_{rCT} as percentage of the prescribed dose (%pD), and (c) gamma analysis. Between 60% and 90% of the treatment field-of-view was imaged in the CBCT in the available datasets. Treatment (black line) and CBCT (purple line) fields-of-view are indicated in (a). Deformable results are clearly better than rigid and extended CBCT. Most striking registration errors, and therefore dose estimation errors, occurred in the skin and airways. The inconsistency in HU is visible for the CBCT results, particularly in the shoulder region. This degrades the accuracy of the dose estimation in a part of the high dose region and spinal canal.

TABLE III. Similarity between dose distributions [deformable (D_{DIR}), rigid-only (D_{RIG}), and extended CBCT (D_{CBCT})] and gold-standard (replan CT) within different regions of interest: mean values (and standard deviation) for DD (2% pass-percentage and mean absolute value) and gamma tests.

		Dose difference (DD) test		
Region of interest	Method	Pass-percentage (%)	Mean test value (%pD)	Gamma test (2%/2mm criterion) Pass-percentage (%)
Treatment FoV	D_{DIR}	87.0 (±6.4)	1.6 (±1.0)	94.3 (±5.4)
	D_{RIG}	75.6 (±4.2)	3.9 (±0.8)	84.7 (±3.3)
	D_{CBCT}	78.5 (±1.0)	2.0 (±0.5)	90.5 (±2.5)
CBCT FoV	D_{DIR}	90.0 (±0.9)	1.2 (±0.2)	97.1 (±1.1)
	D_{RIG}	74.2 (±3.0)	4.4 (±0.8)	83.9 (±2.2)
	D_{CBCT}	79.6 (±8.0)	1.6 (±0.5)	92.6 (± 4.0)
Nonimaged treatment FoV	D_{DIR}	86.0 (±10.5)	1.7 (±1.7)	92.1 (±8.2)
	D_{RIG}	84.1 (±8.7)	2.1 (±1.3)	90.4 (±6.7)
	D_{CBCT}	84.1 (±8.5)	2.0 (±1.3)	90.5 (±6.6)
95% isodose volume	D_{DIR}	93.4 (±8.1)	0.7 (±0.2)	97.1 (±4.3)
	D_{RIG}	67.8 (±6.8)	2.1 (±0.6)	80.0 (±6.2)
	D_{CBCT}	83.7 (±4.5)	1.2 (±0.2)	90.3 (±4.1)

The DD inside the OARs are most relevant clinically (Fig. 7). D_{DIR} dose-differences are clinically insignificant inside OARs, and the results found are superior to those from other dose estimation approaches. The poor image quality of the CBCT in the inferior direction (i.e., neck and shoulders) is responsible for the inferiority of D_{CBCT} in comparison with D_{DIR}. This affects both the dose estimation in the high dose region (Table III and Fig. 6) and in the spinal canal (Fig. 7). The inconsistency in HU is less problematic in the remaining OARs.

3.C. Propagation of structures and "dose of the day"

Figure 8 contains DVHs calculated using (i) D_{rCT} and manually drawn structures on the rCT, (ii) D_{DIR} and the same manual structures, and (iii) D_{DIR} and structures warped from the pCT. Measures of overlap obtained for OARs show that although the volumes are similar the differences can be non-negligible in the DVHs. The mean DSC obtained was 0.810 ± 0.044, 0.822 ± 0.062, 0.760 ± 0.048, and 0.770 ± 0.010, for the brainstem, spinal canal, left parotid, and right parotid,

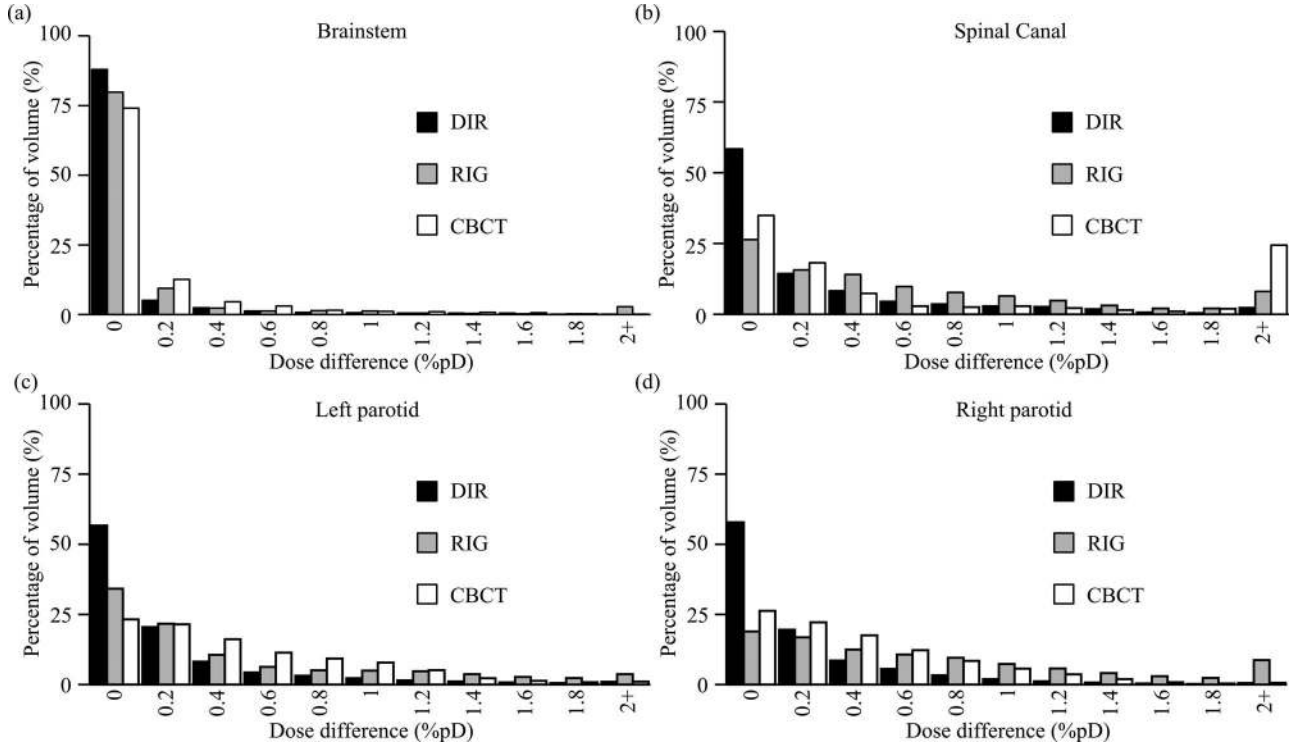

FIG. 7. Dose difference: distribution of values (as percentage of the prescribed dose,%pD), for different OARs and dose calculations.

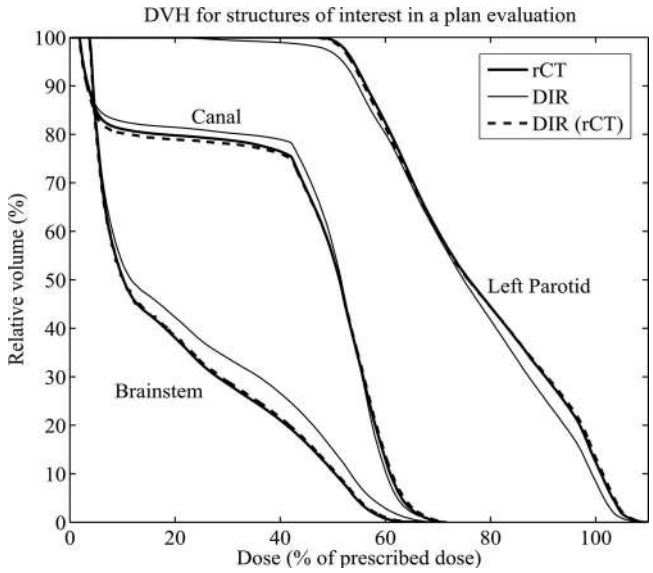

FIG. 8. DVH for different OARs using D_{rCT} and manually drawn structure (rCT), D_{DIR} and structures warped from the pCT (DIR), and D_{DIR} and manually drawn structures [DIR(rCT)].

respectively. From Fig. 8 it can be seen that differences in DVHs were mainly due to differences in the OARs definition (manual vs warped) and not due to differences in dose estimation (D_{rCT} vs D_{DIR}). The same trend was found for the errors in estimating the maximum and mean doses to an OAR (ΔD_{max} and ΔD_{mean}). Using D_{DIR} combined with manually drawn structures on the rCT the mean value obtained for ΔD_{mean} was 0.1% ± 0.1% of the prescribed dose (pD) (range: 0.0%–0.3%pD), while for ΔD_{max} was 0.3% ± 0.2%pD (range: 0.0%–0.6%pD). However, using the warped structures these errors increased to 2.4% ± 2.1%pD (range: 0.3%–7.8%pD) and 1.5% ± 1.6%pD (range: 0.1%–6.2%pD), respectively.

4. DISCUSSION

Regarding the geometric evaluation, all metrics showed an improvement when comparing deformable to rigid registration, up to a relative improvement of 80%. The values found for DSC are comparable to the ones obtained by Castadot *et al.* using CT-CT DIR.[36] DT metrics and CoM values were comparable to image resolution. Combining the DSC, DT, and CoM we can evaluate the ability of the DIR method to map identical structures between the CT and CBCT datasets. However, each of these quantities can be misleading on its own. For example, DSC is inherently bigger for larger structures, such as the external contours, and in this case DT is a better measure of similarity between features.

One of the main limitations of our geometric evaluation is not including localization of anatomical landmarks. Anatomical landmarks were not used in this study due to the difficulty detected by our clinical expert in consistently identifying points in a CBCT image. The uncertainty in landmark locations could produce misleading accuracy results, so we opted to only use structures in the geometric evaluation. Furthermore, we consider that for our current goal of calculating the "dose of the day" accurate point-to-point mapping is not required.

The method presented allows for accurate dose calculations, comparable to doses recalculated on a replan CT and superior to both our current clinical approach and dose calculations on the CBCT (with extended FoV). CBCT images include larger amounts of scattering than CT, resulting in larger variation in HU values that limit the HU calibration and reliability.[1] The CBCT calibrations are done using a small phantom which provides consistent results in such a small FoV. However, for larger volumes the calibration is no longer consistent which has a considerable impact in dose calculations. Figure 6 shows the effect in dose estimation of such inconsistency in HU in the neck and shoulders region. Imaging larger volumes result in increased scatter and reduced transmission. The increase in scatter introduces nonuniformities and additional quantum noise to the reconstructed image.[37] This indicates the need for more specific and appropriate calibration phantoms for CBCT, which should cover the size of the treatment region. The choice of phantom is crucial as others showed different phantoms result in very different relative electron density calibration curves, and particularly the Catphan may not be the most appropriate due to issues with its bone-equivalent material.[18] While we think our results are indicative of how reliable CBCT currently is for direct dose calculations, it was not in the scope of this paper to optimize treatment planning on CBCT images. Our imaging protocol was not optimized for that purpose, and so the calculations were clearly suboptimal. In our opinion calculating dose distributions directly on CBCT images is still an active area of research and the fact that specialized calibrations and optimizations are required is a current disadvantage of such methods. The deteriorated image quality of CBCT leads to serious concerns about its reliability for direct dose calculations. CT is still far superior to CBCT for treatment planning, and DIR is a good interim solution for ART until CBCT data are directly usable.

Our results show promise to obtain dosimetric information even outside the CBCT FoV. The interpolation of the information outside the FoV allows performing dose calculations even when the CBCT FoV is smaller than the treatment FoV. Although we do propose a method for estimating the transformation, and hence the anatomy, outside of the CBCT FoV, we do not claim this will always give trustworthy results. If there is significant deformation outside the FoV then our method will not be able to recover this. Such deformations occurred for one of the patients included in our study where the CBCT field of view did not extend far enough in the inferior direction. Further research will be required to study the validity of our approximation outside the on-board imaging. For future clinical applications, the imaged region must be selected properly to minimize possible out of field errors on critical regions of the individual patient. For example, if the major concern is the dose given, to the brainstem, then the brainstem should be imaged. If target coverage is more important, the high dose region should be properly captured. Informing the imaging procedures will be even more important for bigger patients and/or tumors.

Figure 8 shows how structure delineation has an important impact in plan evaluation. Structure contours deviations explain the differences in DVHs and mean/maximum doses to OARs. The overlap found between OARs is similar to values reported by Tsuji *et al.* for CT-CT DIR.[8] Visually we find that most discrepancies in spinal canal and brainstem are actually due to differences in defining the extent of these organs in the superior direction in the different scans. Generating appropriate structure delineations for ART is an important and on-going area of research,[8,21,24] which is beyond the scope of this paper. In future applications of the tool presented and validated here, deformed structures will be used as a starting point to speed up the evaluation process, but will likely require manual verification and editing to be used clinically. Extra care must be taken if modifying targets during ART. Even though authors suggest the use of DIR to monitor tumor shrinkage,[38] in our case warping target volumes may not be appropriate as they are usually not visible in CBCT imaging. Also, even if the gross tumor volume (GTV) shrinkage is visible, there is no evidence that microscopic proliferation has shrunk in the same proportion. Guidelines for target propagation are still being developed by our group and others. Including routine functional imaging, such as magnetic resonance imaging (MRI), in the ART workflow may provide not only a solution for target propagation but also early evidence of the patient response to the treatment.[39,40]

We have validated the use of DIR for calculating the "dose of the day," but this does not necessarily guarantee correct point-to-point matching. Point-to-point matching is important when handling dose remapping and summation, but is very difficult to validate because the true correspondence is unknown.[21] Dose remapping and summation is very sensitive to the actual displacement map since small errors in deformation can result in significant changes in dose at points in high dose gradient regions.[41] Additionally, warping the "dose of the day" back to the original pCT for summation requires the inverse of the pCT-CBCT transformation. Therefore, symmetric and diffeomorphic registrations are desired to ensure invertibility and remove bias from the direction of the registration. Such approaches are currently being investigated,[31] and preliminary results indicate that our DIR framework can be successfully used for dose summation.

Further work will also focus on measuring the accuracy of the deformation maps and further improvements of the registrations. One of the sources of errors in DIR is the inherent deformation of bony elements, which physically can only move rigidly. Rigidity penalty terms, that constrain the registration to be rigid in regions of interest, are desired in a realistic deformable registration algorithm to increase the accuracy of the tissue mapping.[42] Other similarity measures can also be investigated to improve the robustness of the registrations.[43,44]

The patients included in this study had considerable anatomical changes during the course of their treatment. We consider the tests applied to our registration quite severe as those patients were selected from the group of identified sensitive cases treated in our practice. The registrations were particularly challenging for the dose comparisons since not only anatomical changes but also different positioning systems had to be reproduced. For this reason we expect our routine clinical cases to be less demanding.

The initial clinical application of our method will be weekly offline calculations of the "dose of the day" to help inform the decision of whether the current plan is still acceptable. At this point if a plan is found to be unacceptable our current replan pathway will be followed. Replanned patients will be used on further validation to support the effectiveness and efficiency of the proposed method. With more patients it may be possible to understand the relationship between DIR and dose errors, which could be used to establish quick and easy methods for detecting regions where DIR errors are significant from a dose calculation point of view. On a longer term the aim is for our tool to be employed for the replan procedure itself and remove the need for acquiring a new CT when a new immobilization is not necessary. The final aim is to enable the implementation of a controlled "dose-driven" ART approach that can be built into the patient pathway: to perform routine online modifications to the treatment plan based on the dose that has already been delivered.

5. CONCLUSIONS

This work presents a proof-of-principle of the application of an in-house developed deformable registration for ART purposes. We have developed, optimized, and evaluated a CT-to-CBCT DIR and our experiments have demonstrated that using a pCT scan deformed to match a CBCT scan results in similar dose calculations to those performed on a new CT scan. The dose differences were clinically acceptable, and our method provided dose estimation closer to the gold standard than calculations in a rigidly aligned pCT and extended CBCT. The results obtained support the use of nonrigid registration and provide further evidence in the challenging objective of validating deformable registration for routine clinical use. The work here presented is a first step into a full implementation of a "dose-driven" online ART.

ACKNOWLEDGMENTS

The authors would like to thank Pankaj Daga, Gergely Zombori, and Matt Clarkson for all the support with NiftyReg and Phil Davies, Rachel Bodey, Chris Stacey, and Ivan Rosenberg for the clinical input. C.V. was funded by Fundação para a Ciência e a Tecnologia (FCT) grant SFRH/BD/76169/2011, co-financed by ESF, POPH/QREN and EU. J.M. was supported by the EPSRC Intelligent Imaging Program Grant EP/H046410/1. M.M. and S.O. were supported by the UCLH/UCL NIHR CBRC grant 168.

[a]Author to whom correspondence should be addressed. Electronic email: catarina.veiga.11@ucl.ac.uk

[1]M. Stock, M. Pasler, W. Birkfellner, P. Homolka, R. Poetter, and D. Georg, "Image quality and stability of image-guided radiotherapy (IGRT) devices: A comparative study," Radiother. Oncol. **93**(1), 1–7 (2009).

[2]I. Fotina, J. Hopfgartner, M. Stock, T. Steininger, C. Lütgendorf-Caucig, and D. Georg, "Feasibility of CBCT-based dose calculation: Comparative analysis of HU adjustment techniques," Radiother. Oncol. **104**(2), 249–256 (2012).

[3]J. R. McClelland, S. Hughes, M. Modat, A. Qureshi, S. Ahmad, D. B. Landau, S. Ourselin, and D. J. Hawkes, "Inter-fraction variations in respiratory motion models," Phys. Med. Biol. **56**(1), 251–272 (2011).
[4]E. K. Hansen, M. K. Bucci, J. M. Quivey, V. Weinberg, P. Xia, "Repeat CT imaging and replanning during the course of IMRT for head-and-neck cancer," Int. J. Radiat. Oncol., Biol., Phys. **64**(2), 355–362 (2006).
[5]D. Yan, F. Vicini, J. Wong, and A. Martinez, "Adaptive radiation therapy," Phys. Med. Biol. **42**(1), 123–132 (1997).
[6]Q. J. Wu, T. Li, Q. Wu, and F. F. Yin, "Adaptive radiation therapy: Technical components and clinical applications," Cancer J. **17**(3), 182–189 (2011).
[7]L. Xing, J. Siebers, and P. Keall, "Computational challenges for image-guided radiation therapy: Framework and current research," Semin. Radiat. Oncol. **17**, 245–257 (2007).
[8]S. Y. Tsuji, A. Hwang, V. Weinberg, S. S. Yom, J. M. Quivey, and P. Xia, "Dosimetric evaluation of automatic segmentation for adaptive IMRT for head-and-neck cancer," Int. J. Radiat. Oncol., Biol., Phys. **77**(3), 707–714 (2010).
[9]P. Castadot, J. A. Lee, X. Geets, and V. Grégoire, "Adaptive radiotherapy of head and neck cancer," Semin. Radiat. Oncol. **20**, 84–93 (2010).
[10]D. L. Schwartz and L. Dong, "Adaptive radiation therapy for head and neck cancer – Can an old goal evolve into a new standard," J. Oncol. (2011).
[11]C. Lee, K. M. Langen, W. Lu, J. Haimerl, E. Schnarr, K. J. Ruchala, G. H. Olivera, S. L. Meeks, P. A. Kupelian, T. D. Shellenberger, and R. R. Mañon, "Evaluation of geometric changes of parotid glands during head and neck cancer radiotherapy using daily MVCT and automatic deformable registration," Radiother. Oncol. **89**(1), 81–88 (2008).
[12]J. L. Barker, A. S. Garden, K. K. Ang, J. C. O'Daniel, H. Wang, L. E. Court, W. H. Morrison, D. I. Rosenthal, K. S. Chao, S. L. Tucker, R. Mohan, and L. Dong, "Quantification of volumetric and geometric changes occurring during fractionated radiotherapy for head-and-neck cancer using an integrated CT/linear accelerator system," Int. J. Radiat. Oncol., Biol., Phys. **59**(4), 960–970 (2004).
[13]S. Marzi, P. Pinnarò, D. D'Alessio, L. Strigari, V. Bruzzaniti, C. Giordano, G. Giovinazzo, and L. Marucci, "Anatomical and dose changes of gross tumour volume and parotid glands for head and neck cancer patients during intensity-modulated radiotherapy: Effect on the probability of xerostomia incidence," Clin. Oncol. (R. Coll. Radiol.) **24**(3), e54–e62 (2012).
[14]D. L. Schwartz, A. S. Garden, S. J. Shah, G. Cheonowski, S. Seipal, D. I. Rosenthal, Y. Chen, Y. Zhang, L. Zhang, P. F. Wong, J. A. Garcia, K. Kian Ang, and L. Dong, "Adaptive radiotherapy for head and neck cancer – Dosimetric results from a prospective clinical trial," Radiother. Oncol. **106**(1), 80–84 (2013).
[15]D. L. Schwartz, A. S. Garden, J. Thomas, Y. Chen, Y. Zhang, J. Lewin, M. S. Chambers, and L. Dong, "Adaptive radiotherapy for head-and-neck cancer: Initial clinical outcomes from a prospective trial," Int. J. Radiat. Oncol., Biol., Phys. **83**(3), 986–993 (2012).
[16]A. Richter, Q. Hu, D. Steglich, K. Baier, J. Wilbert, M. Guckenberger, and M. Flentje, "Investigation of the usability of conebeam CT data sets for dose calculation," Radiat. Oncol. **16**, 3–42 (2008).
[17]K. Usui, Y. Ichimaru, Y. Okumura, K. Murakami, M. Seo, E. Kunieda, and K. Ogawa, "Dose calculation with a cone beam CT image in image-guided radiation therapy," Radiol. Phys. Technol. **6**(1), 107–114 (2013).
[18]H. Guan and H. Dong, "Dose calculation accuracy using cone-beam CT (CBCT) for pelvic adaptive radiotherapy," Phys. Med. Biol. **54**(20), 6239–6250 (2009).
[19]Y. Yang, E. Schreibmann, T. Li, C. Wang, and L. Xing, "Evaluation of on-board kV cone beam CT (CBCT)-based dose calculation," Phys. Med. Biol. **52**(3), 685–705 (2007).
[20]H. Zhong, J. Kim, and I. J. Chetty, "Analysis of deformable image registration accuracy using computational modelling," Med. Phys. **37**(3), 970–979 (2010).
[21]T. Zhang, Y. Chi, E. Meldolesi, and D. Yan, "Automatic delineation of on-line head-and-neck computed tomography images: Toward on-line adaptive radiotherapy," Int. J. Radiat. Oncol., Biol., Phys. **68**(2), 522–530 (2007).
[22]J. D. Lawson, E. Schreibmann, A. B. Jani, and T. Fox, "Quantitative evaluation of a cone-beam computed tomography-planning computed tomography deformable image registration method for adaptive radiation therapy," J. Appl. Clin. Med. Phys. **8**(4), 96–113 (2007).
[23]J. Hou, M. Guerrero, W. Chen, and W. D. D'Souza, "Deformable planning CT to cone-beam CT image registration in head-and-neck cancer," Med. Phys. **38**(4), 2088–2094 (2011).
[24]M. Peroni, D. Ciardo, M. F. Spadea, M. Riboldi, S. Comi, G. Baroni, and R. Orecchia, "Automatic segmentation and online virtualCT in head-and-neck adaptive radiation therapy," Int. J. Radiat. Oncol., Biol., Phys. **84**(3), e427–e433 (2012).
[25]T. Lo, Y. Yang, E. Schreibmann, T. Li, and L. Xing, "Mapping electron density distribution from Planning CT to cone-beam CT (CBCT): A novel strategy for accurate dose calculation based on CBCT," Int. J. Radiat. Oncol., Biol., Phys. **63**(1), S507 (2005).
[26]S. Ourselin, A. Roche, G. Subsol, X. Pennec, and N. Ayache, "Reconstructing a 3D structure from serial histological sections," Image Vis. Comput. **19**, 25–31 (2001).
[27]D. Rueckert, L. I. Sonoda, C. Hayes, D. L. Hill, M. O. Leach, and D. J. Hawkes, "Nonrigid registration using free-form deformations: Application to breast MR images," IEEE Trans. Med. Imaging **18**(8), 712–721 (1999).
[28]M. Modat, G. R. Ridgway, Z. A. Taylor, M. Lehmann, J. Barnes, D. J. Hawkes, N. C. Fox, and S. Ourselin, "Fast free-form deformation using graphics processing unit," Comput. Methods Programs Biomed. **98**(3), 278–284 (2010).
[29]C. Veiga, J. McClelland, K. Ricketts, D. D'Souza, and G. Royle, "Deformable registrations for head and neck cancer adaptive radiotherapy," *Image-Guidance and Multimodal Dose Planning in Radiation Therapy Workshop of the 15th International Conference on Medical Image Computing and Computer Assisted Intervention (MICCAI)*, Nice, France (2012).
[30]C. Veiga, J. McClelland, S. Moinuddin, K. Ricketts, M. Modat, S. Ourselin, D. D'Souza, and G. Royle, "Towards adaptive radiotherapy for head and neck patients: Validation of an in-house deformable registration algorithm," J. Phys.: Conf. Ser. (in press).
[31]M. Modat, M. J. Cardoso, P. Daga, D. Cash, N. C. Fox, and S. Ourselin, "Inverse-consistent symmetric free form deformation," *Biomedical Image Registration*, edited by B. M. Dawant, G. E. Christensen, J. M. Fitzpatrick, and D. Rueckert, Lecture Notes in Computer Science Vol. 7359 (Springer Berlin Heidelberg, 2012), 79–88.
[32]M. Modat, J. R. McClelland, and S. Ourselin, "Lung registration using the NiftyReg package," in *Medical Image Analysis for the Clinic: A Grand Challenge Workshop proceedings from the 13th International Conference on Medical Image Computing and Computer Assisted Intervention (MICCAI)*, edited by B. van Ginneken, K. Murphy, T. Heimann, V. Pekar, and X. Den (Beijing, China, 2010), pp. 33–42.
[33]G. X. Ding, D. M. Duggan, C. W. Coffey, M. Deeley, D. E. Hallahn, A. Cmelak, and A. Malcolm, "A study on adaptive IMRT treatment planning using kV cone-beam CT," Radiother. Oncol. **85**, 116–126 (2007).
[34]V. Grégoire, P. Levendag, K. K. Ang, J. Bernier, M. Braaksma, V. Budach, C. Chao, E. Coche, J. S. Cooper, G. Cosnard, A. Eisbruch, S. El-Sayed, B. Emami, C. Grau, M. Hamoir, N. Lee, P. Maingon, K. Muller, and H. Reychler, "CT-based delineation of lymph node levels and related CTVs in the node-negative neck: DAHANCA, EORTC, GORTEC, NCIC, RTOG consensus guidelines," Radiother. Oncol. **69**, 227–236 (2003).
[35]D. A. Low, W. B. Harms, S. Mutic, and J. A. Purdy, "A technique for the quantitative evaluation of dose distributions," Med. Phys. **25**(5), 656–661 (1998).
[36]P. Castadot, J. A. Lee, A. Parraga, X. Geets, B. Macq, and V. Grégoire, "Comparison of 12 deformable registration strategies in adaptive radiation therapy for the treatment of head and neck tumors," Radiother. Oncol. **89**, 1–12 (2008).
[37]D. A. Jaffray and J. H. Siewerdsen, "Cone-beam computed tomography with a flat-panel imager: Initial performance and characterization," Med. Phys. **27**(6), 1311–1323 (2000).
[38]W. Lu, G. H. Olivera, Q. Chen, K. J. Ruchala, J. Haimer, S. L. Meeks, K. M. Langen, and P. A. Kupelian, "Deformable registration of the planning image (kVCT) and the daily images (MVCT) for adaptive radiation therapy," Phys. Med. Biol. **51**, 4357–4374 (2006).
[39]H. Kato, M. Kanematsu, O. Tanaka, K. Mizuta, M. Aoki, T. Shibata, T. Yamashita, Y. Hirose, and H. Hoshi, "Head and neck squamous cell carcinoma: Usefulness of diffusion-weighted MR imaging in the prediction of a neoadjuvant therapeutic effect," Eur. Radiol. **19**(1), 103–109 (2009).
[40]H. C. Thoeny, F. De Keyzer, and A. D. King, "Diffusion-weighted MR imaging in the head and neck" Radiology **263**(1), 19–32 (2012).
[41]R. Kashani, M. Hub, J. M. Balter, M. L. Kessler, L. Dong, L. Zhang, L. Xing, Y. Xie, D. Hawkes, J. A. Schnabel, J. McClelland, S. Joshi, Q. Chen, and W. Lu, "Objective assessment of deformable image

registration in radiotherapy: A multi-institution study," Med. Phys. **35**(12), 5944–5953 (2008).

[42]J. Kim, M. Matuszak, J. Balter, and K. Saitou, "An improved rigidity penalty for deformable registration of head and neck images in intensity-modulated radiation therapy," *Proceedings of IEEE International Conference on Automation Science and Engineering* (Seoul, Korea, 2012), pp. 377–382.

[43]W. Birkfellner, M. Stock, M. Figl, C. Gendrin, J. Hummel, S. Dong, J. Kettenbach, D. Georg, and H. Bergmann, "Stochastic rank correlation: A robust merit function for 2D/3D registration of image data obtained at different energies," Med. Phys. **36**(8), 3420–3428 (2009).

[44]P. Cachier, E. Bardinet, D. Dormont, X. Pennec, and N. Ayache, "Iconic feature based nonrigid registration: The PASHA algorithm," Comput. Vis. Image Understanding **89**, 272–298 (2003).